8

# Microcellular Foam Injection Molding Process

Hu Guanghong and Wang Yue
*National Engineering Research Center of Die & Mold CAD,*
*Shanghai Jiao Tong University, Shanghai,*
*China*

## 1. Introduction

In recent years, the polymer resin price is rising due to the petroleum shortage. How to save plastics on the premise to ensure the plastics part quality is one of the research hotspots. Microcellular foam injection molding process is developed in this background. Microcellular foam technology was invented by MIT in the early 1980's [1]. The traditional foaming processes, which produce bubbles larger than 0.25mm, are not feasible due to excessive loss of strength. Thus, the idea was born to create microcellular foam to both save plastics and have reasonable strength.

Generally, microcellular foam process takes advantage of supercritical fluid (SCF) as physical blowing agent. $CO_2$ and $N_2$ are usually used as agent. The microcellular foam parts have uniform cell diameters of 1 to100 microns and cell density of $10^9$ to $10^{15}$ cells per cubic centimeters. Figure 1-1 shows the scanning electron micrographs of microcellular polystyrene sample [2].

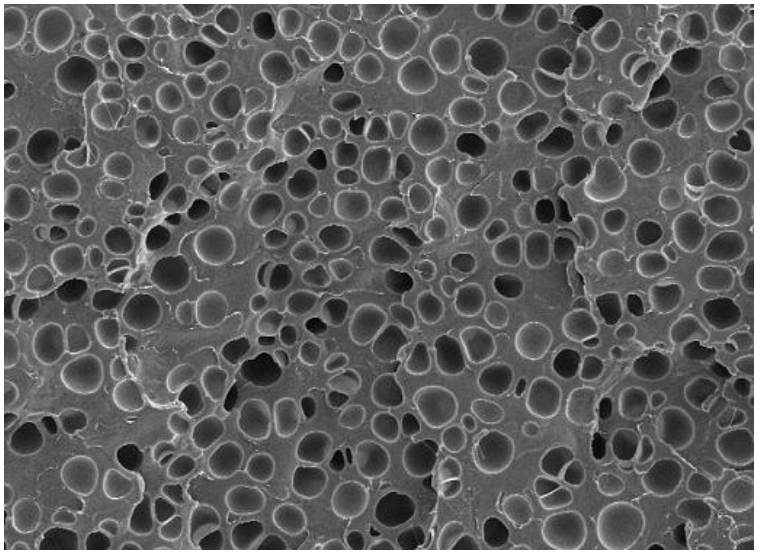

Fig. 1-1. Electron micrographs of microcellular polystyrene scanning sample [2].

Now microcellular foam technology is extended into many other plastics forming process such as extrusion, injection, blowing process. And microcellular foam technology is widely used in the homework appliance, aerospace and auto industry *etc*. In this book, microcellular foam injection molding process is mainly discussed.

### 1.1 Microcellular foam injection process principle

During microcellular foam injection molding process, SCF is injected into the polymer melt. And the single phase of polymer- SCF mixed solution is obtained under certain temperature and pressure. When the mixer is injected into the mold, the pressure of the single-phase solution is dropped from microcellular process pressure (MPP) to atmospheric pressure. The nucleation phenomena occur due to the gas separated out of the mixer. Then these nuclei finally grow up to stable bubbles.

Figure 1-2 shows the microcellular foam injection molding process. And generally the microcellular foam injection molding process is described as following four steps.

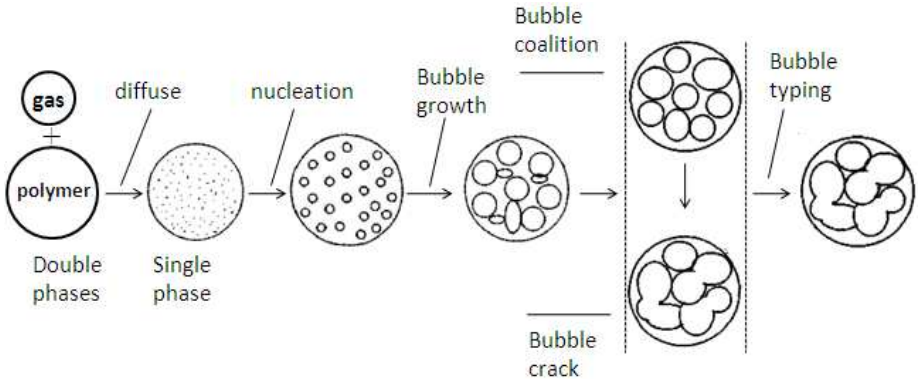


Fig. 1-2. Illustration of microcellular polymer foaming process [3].

**Polymer-SCF single phase generation**

During microcellular foam injection molding process, the supercritical nitrogen ($N_2$) or carbon dioxide ($CO_2$) is injected into plastics injection machine barrel and dissolved into polymer melt. Then a single phase polymer-SCF solution is generated under the definite temperature and pressure. In this stage, the concentration of SCF is determined by saturation, microcellular process pressure (MPP) and the mixer temperature. These parameters also significantly affect the final bubbles size.

**Homogeneous nucleation**

Theoretically, only when the polymer-SCF mixer is in the thermodynamics equilibrium and millions of nuclei are generated at the same time, homogeneous nucleation will be possible. When the polymer-SCF single phase mixer is injected into mold cavity, the mixer pressure is changed from MPP to the atmospheric pressure. Thus a rapid pressures unloading occurs. Then, SCF separates from the single phase mixer, and a large number of nuclei are generated. With the nucleus growing, free energy of the mixer is also increasing. Only when the nucleus size is bigger than the critical one, the nucleus will be stable. And the bubble

growing can be possible. Thus, the mixer temperature, MPP and SCF concentration affect the nuclei process and the final nucleus density.

**Bubbles growth**

When millions of nuclei are generated and the nucleus is stable, the bubbles growth start. SCF concentration of mixer is higher than the SCF concentration inside bubbles. Due to the concentration difference SCF in the mixer enters the bubbles. And the gas bubbles grow up. Until the SCF concentration inside bubbles equals to the outside one or the melt is frozen, the gas bubbles will keep growing up. Thus, the final bubble morphology is determined by the SCF concentration and injection process parameters.

**Product typing**

Along with mold cooling, the melt temperature is decreased and the melt freezes up. The bubbles stop growing up. And the shape of part is fixed.

From above microcellular foam injection molding process, the properties of microcellular foam injection molding parts are determined by nucleation process and final bubble morphology besides tradition injection process condition such as part shape, the kind of polymer, mold structure, process parameters. Thus microcellular foam injection molding process has distinct characters comparing to the traditional plastics injection.

### 1.2 Microcellular foam injection molding process characters

Due to SCF injected into the polymer melt, it is great affect the polymer melt viscosity, injection molding process cycle, part weight, mechanical properties and surface quality *etc*.

#### 1.2.1 Melt viscosity

Due to the SCF dissolved in the polymer melt, the glass transition temperature of polymer melt becomes lower. So the polymer viscosity is decreased and the melt fluidity becomes better. Thus, the required injection pressure is lower than tradition injection and the requirement of injection machine properties is less. Figure 1-3 shows the effect of SCF on the PA, PBT melt viscosity [4]. The results indicate that the viscosity is decreased after the SCF is added.

It should be pointed out that the effect of SCF on the polymer viscosity is determined by the polymer kind and filler. Because SCF can't be dissolved into the filler, it will not affect the filler viscosity. Thus comparing to the pure polymer, the effect of SCF on the viscosity of polymer with filler is less.

#### 1.2.2 Injection cycle time

Microcellular foam injection molding technology can reduce the cycle time. The reasons mainly include: (1). because the gas in the bubbles can provide the packing pressure, the packing and holding phase can be eliminated. (2). When the millions of nucleus are generated and bubbles grow up, they are all endothermic reaction. So the cooling time is saved. (3). Due to the bubbles in the part, the part weight is reduced. The cooling time is also saved. (4). The lower viscosity means higher filling speed. The filling time becomes short. Generally 20%~50% cycle time can be saved by microcellular foam injection molding

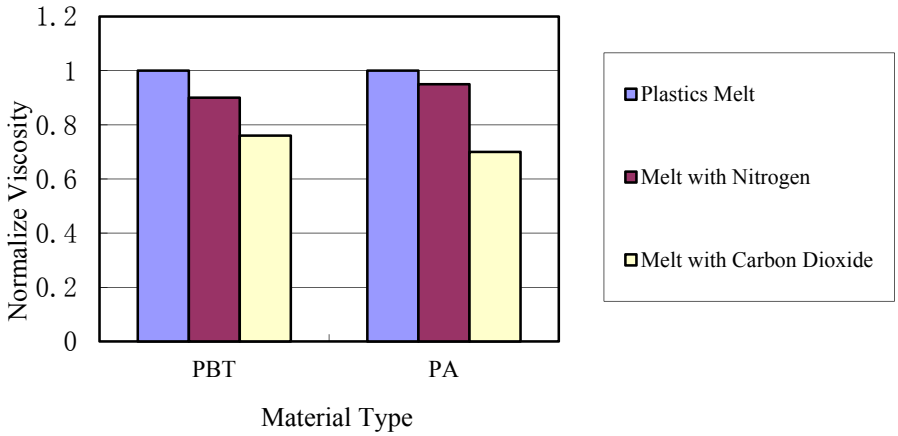


Fig. 1-3. Effect of SCF on melt viscosity [4].

process. Figure 1-4 shows the comparison between microcellular foam injection molding process cycle and traditional injection one.

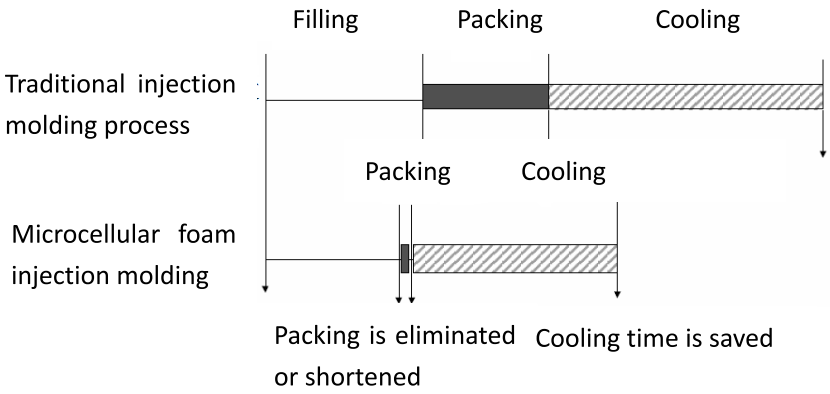


Fig. 1-4. Comparison between microcellular foam injection molding process cycle and traditional injection process.

### 1.2.3 Part weight

Due to the bubbles in the part, the polymer obviously can be saved. Generally the part weight can be reduced as 0.5mm thickness weight by microcellular foam injection molding process. At the same time, all kinds of polymer, even including the high temperature polyphenylsulfone, can be formed by this technology. The effect of microcellular foam injection molding process on the weight reduction is shown in the Table 1-1.

| Polymer | Part thickness(mm) | Weight reduction (%) |
|---|---|---|
| Polyphenylsulfone | 5 | 50 |
| PS | 1.5 | 30 |
| Acetal | 1.5 | 15 |
| PET | 5 | 30 |
| TPE | 1.5 | 20 |
| PP (30%Talc) | 2.1 | 25 |
| HDPE | 5 | 60 |
| PC/ABS | 2.1 | 23 |
| PA | 1.2 | 9 |
| PA(40% Filler) | 2 | 15 |
| PC | 7.2 | 45 |

Table 1-1. Effect of microcellular foam process on weight reduction [5].

### 1.2.4 Part mechanical properites

Also, the parts mechanical properties are changed due to the bubbles. The former researches indicate that the part bend strength of microcellular foam polymer is almost same as the solid polymer. Thus microcellular foam technology can be used to produce the inner structure part. However it is quite different situation for the part tensile strength. The tensile property data shows that the tensile strength of microcellular foams decreases in proportion to the foam density. It means that a 50% relative density foam can be expected to have 50% of the strength of the solid polymer. To the part impact strength, it is more sensitive to variation from polymer to polymer. And the results cannot be generalized. However the Gardner impact strength of PVC foam experiment results show that the impact strength decreases linearly with foam density. It should be pointed out that the impact strength of

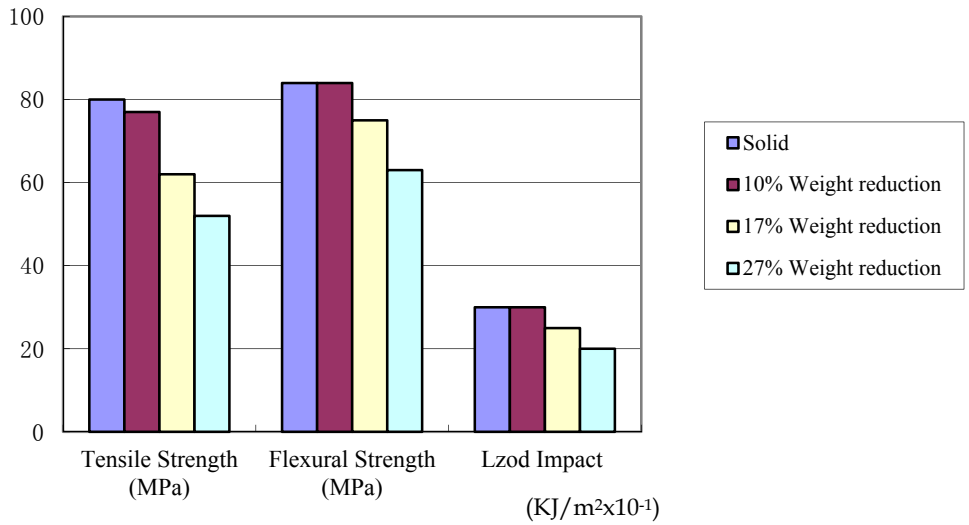


Fig. 1-5. PBT mechanical properties on the different weight reduction ratio.

polymer added filler is decreased less than one without any filler. The main reason is that the filler properties and content percent great affect the part impact strength. And SCF has no effect on the fillers[6-13]. Figure 1-5 shows the bend strength, tensile strength and impact strength of PBT (30% GF) on the solid polymer and different weight reduction ratio. The results present the almost same rules as above.

### 1.2.5 Surface quality

As said above, microcellular foam injection molding process presents nice formability and lots of advantages. But still due to SCF, the part surface quality is worse than tradition process. Typical surface defects are swirl marks, silver streak, surface blistering, post-blow and large surface roughness. These defects limit the application scope of microcellular foam injection process seriously. Figure 1-6 shows main surface defects of microcellular foam injection molding parts.

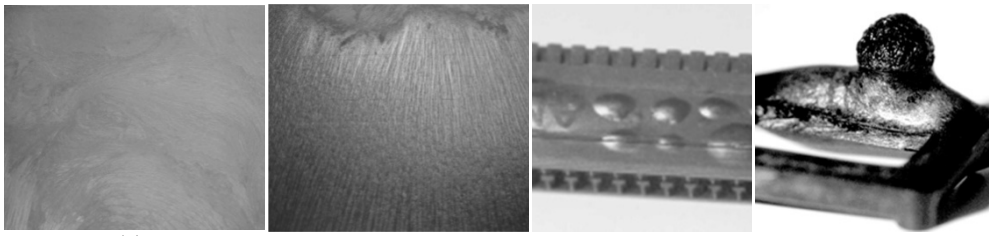

(a) (b) (c) (d)

Fig. 1-6. Surface defects of microcellular foam injection molding parts (a) swirl mark[14]; (b) silver streak[14]; (c) surface blistering[15]; (d) post-blow[15].

**Swirl marks**

Grooves on the part surface are caused by the trapped gas on the mold surface when the polymer-SCF mixer begins to solidify. And the area of grooves surface shows positive correlation. The shape of these grooves is slender along the flow direction, and the aspect ratio of grooves indicates the size of shear strength which is caused by the polymer-SCF mixer filling behavior in the mold cavity. Swirl marks are these grooves whose shapes are curled (see Figure 1-5a).

Yoon propose that the glass transition temperature (for the amorphous polymer) or the melt temperature (for the crystalline polymer) is one of the important effect factors on the swirl mark forming [16]. Zhang YT points out that swirl marks always appear near the gate [17]. While the polymer-SCF mixer is injected into mold cavity, many parameters in different mold cavity area are varied. Generally near the gate, the temperature is higher, viscosity of the polymer-SCF is smaller, and melt strength is lower. So the gas near the gate is easy to diffuse to the mixer surface, and the bubbles near the surface break up easily.

**Silver streak**

Silver streak is a defect that shows silver gloss in the sunlight (see Figure 1-5b). Silver streak of microcellular foam injection parts shows two different appearances. One is called silver thread because its boundary looks like a thread. This defect is caused by the broken bubbles at the surface of melt. The other is called silver strip because it looks like a strip which

parallels the flow direction. The difference between them is that there are no broken bubbles at the surface to the latter.

Michaeli and Cramer point out that the silver streaks are flow marks of the polymer-SCF mixer on the mold cavity surface. It's the shear deformation of the bubbles that are close to the surface. Because of different bubble sizes, the depth of silver threads is different and then the parts surface roughness is different. Compared with silver trips, silver threads will cause larger surface roughness [18].

**Surface blistering**

When many tiny bubbles converge at the part thin wall place, it makes a thin polymer layer separate from the main part body. This phenomenon is called surface blistering. (see Figure 1-5c). Surface blistering most likely appears in the parts that are made by crystalline polymer without filler such as POM. Surface blistering can be eliminated by adjusting the microcellular foam injection process parameters and improving the mold design.

**Post-blow**

Post-blow is similar to the internal blistering and always appears at the place of hot spots (see Figure 1-5d). The post-blow defect is caused by following two factors. One is that the cooling is not enough at the hotspots; the other is that too much gas enters the some certain bubbles due to the high SCF concentration and form some large size bubbles. When the pressure inside the bubbles is higher than the outside one, the post-blow will happen. So the method to eliminate this defect is to enhancing cooling at the hot spots and adjusting SCF concentration.

**Surface roughness**

In addition to the above serious defects, surface roughness is another problem that limits the application scope of microcellular foam injection molding process. During bubbles growing up, some small bubbles break up near the surface, and the gas is trapped on the mold surface when the polymer-SCF mixer begins to solidify. So the surface roughness of microcellular foam injection parts is higher than that of traditional injection parts.

## 2. Microcellular foam injection molding theories

According to above chapters, all the advantages and disadvantages are all caused by the SCF injected into the polymer melt. Before introduction microcellular foam injection molding theories, supercritical fluid is firstly discussed.

### 2.1 Supercritical fluid

Supercritical fluid is any substance at certain temperature and pressure above its critical point, where distinct liquid and gas phases do not exist. It can effuse through solids like gas, and dissolve materials like liquid. In addition, close to the critical point, small changes in pressure or temperature result in large changes in density, and allowing many properties of supercritical fluid to be "fine-tuned". Supercritical fluids are suitable as a substitute for organic solvents in a range of industrial and laboratory processes. Carbon dioxide and nitrogen are the most commonly used supercritical fluids for microcellular foam injection molding. Figure 2-1 shows the Carbon dioxide pressure-temperature phase diagram.

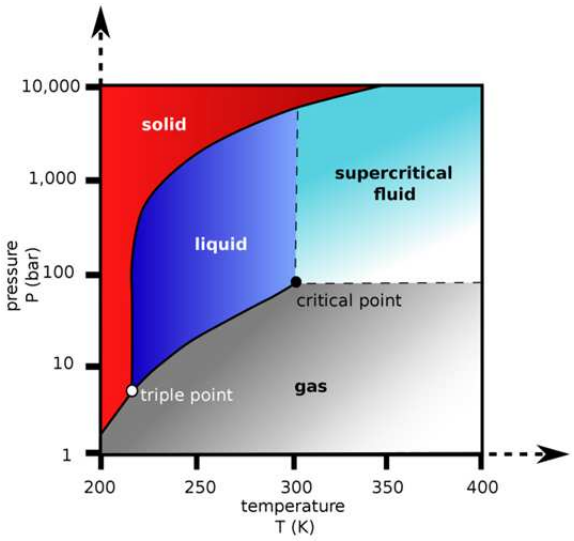


Fig. 2-1. Carbon dioxide pressure-temperature phase diagram [30].

In Figure 2-1, the boiling separates the gas and liquid region and ends in the critical point, where the liquid and gas phases disappear to become a single supercritical phase.

In general terms, supercritical fluids have properties between those of gas and liquid. In the Table 2-1, the critical properties are shown for some components, which are commonly used as supercritical fluids.

| Solvent | Molecular weight g/mol | Critical temperature K | Critical pressure MPa (atm) | Critical density g/cm3 |
|---|---|---|---|---|
| $CO_2$ | 44.01 | 304.1 | 7.38 (72.8) | 0.469 |
| $N_2$ | 28 | 126.2 | 3.4 (33.6) | -- |
| $H_2O$ | 18.015 | 647.096 | 22.064 (217.755) | 0.322 |
| $CH_4$ | 16.04 | 190.4 | 4.60 (45.5) | 0.162 |
| $C_2H_6$ | 30.07 | 305.3 | 4.87 (48.1) | 0.203 |
| $C_3H_8$ | 44.09 | 369.8 | 4.25 (41.9) | 0.217 |
| $C_2H_4$ | 28.05 | 282.4 | 5.04 (49.7) | 0.215 |
| $C_3H_6$ | 42.08 | 364.9 | 4.60 (45.4) | 0.232 |
| $CH_3OH$ | 32.04 | 512.6 | 8.09 (79.8) | 0.272 |
| $C_2H_5OH$ | 46.07 | 513.9 | 6.14 (60.6) | 0.276 |
| $C_3H_6O$ | 58.08 | 508.1 | 4.70 (46.4) | 0.278 |

Table 2-1.Critical properties of various solvents [30].

### 2.1.1 Nitrogen vs carbon dioxide

Both nitrogen and carbon dioxide are widely used in microcellular foam processing. However, the choice of blowing agent affects the final parts bubble morphology. Therefore, the choice should be made depending on what microcellular foam bubble morphology is desired rather than on ease of use or blowing agent costs.

Table 2-2 shows that carbon dioxide generally has much greater solubility in molten polymers than nitrogen. It indicates that more carbon dioxide can be added to the polymer melt in microcellular foam processing than nitrogen. The result of higher blowing agent concentration in the polymer melt means more density reduction. Table 2-2 shows $CO_2$ and $N_2$ maximum solubility in different polymer melt at 200℃temperature and 27.6MPa pressure[1].

| Polymer | Carbon dioxide (%) | Nitrogen (%) |
|---|---|---|
| PE | 14 | 3 |
| PP | 11 | 4 |
| PS | 11 | 2 |
| PMMA | 13 | 1 |

Table 2-2. Estimated Maximum Gas Solubility at 200℃/27.6MPa[1].

However, because of the similar diffusion rates of nitrogen and carbon dioxide in polymers melt, as shown in the Table 2-3, nitrogen lends to generate smaller cells at the same concentration in polymer melt than carbon dioxide. And the driving force of nitrogen to devolve from the polymer-SCF single phase solution is greater than carbon dioxide. Thus more nucleation sites can be formed in the polymer-nitrogen mixer. Because the diffusion rates are similar, all nucleation sites grow at the same rate whatever nitrogen or carbon dioxide is the blown agent. Thus nitrogen has smaller cell sizes.

| Polymer | Carbon Dioxide($cm^2/s$) | Nitrogen($cm^2/s$) |
|---|---|---|
| PS | $1.3\times10^{-5}$ | $1.5\times10^{-5}$ |
| PE | $2.6\times10^{-6}$ | $8.8\times10^{-7}$ |
| HDPE | $2.4\times10^{-5}$ | $2.5\times10^{-5}$ |
| LDPE | $1.1\times10^{-4}$ | $1.5\times10^{-4}$ |
| PTFE | $7.0\times10^{-6}$ | $8.3\times10^{-6}$ |
| PVC | $3.8\times10^{-5}$ | $4.3\times10^{-5}$ |

Table 2-3. Estimated Diffusion Coefficient at 200℃ [1].

### 2.2 Nucleation theory

#### 2.2.1 Theories of nucleation processing

The nucleation theory was established by Gibbs in early 20th century. Colton [31] proposed the classic nucleation theory, which should be classified into three types: the homogeneous nucleation, heterogeneous nucleation and cavity nucleation.

The main concern of classical nucleation theory is a thermodynamic description of initial stage of nucleation from embryo to nucleus with a little larger size than the critical one.

Homogeneous nucleation occurs in single phase solution system that has no impurity. During the pressure unloading process, every gas molecules will be a nucleation point. So theoretically the largest nucleation density and the smallest bubble size in the final parts will be obtained by homogeneous nucleation. However, due to the purity system, it need more energy to overcome the "energy barrier" to create stable and effective nucleus. Thus there should be more super saturation in the polymer-SCF system.

Heterogeneous nucleation considers that there will be some impurity dispersed in the polymer-SCF mixer. Because there will be more interfacial energy at the impurity solid surface, the nucleation driving force at the impurity solid surface is bigger than the other places. It means that less free energy should be overcome for the nucleus generation. Compared with homogeneous nucleation, heterogeneous nucleation is easier to generate nuclei.

Cavity nucleation is that many nuclei are generated at the cavity places. The gas will be absorbed in the cavity by the nucleating agent or any other micro impurities. Polymer melt can't enter the split wedges at the roughness surface. However the gas will be trapped in these split wedges. During the nucleation process, the gas is tended to enter these cavities to form the nuclei. At the same time, these cavities can save the nucleation energy. And then the stable nucleus can be generated easily.

In this chapter, based on the classical homogeneous nucleation, the microcellular foam nucleation theory is introduced.

### 2.2.2 Homogeneous nucleation

**Classical homogeneous nucleation [19]**

The main concern of classical homogeneous nucleation theory has been a thermodynamic description of initial stage of nucleation from embryo to nucleus. When the thermodynamic equilibrium is broken and the change of free energy of mixer is more than the "energy barrier", the phase transition occurs and the nuclei are generated. When the nuclei are bigger than the critical one, the nuclei become stable and continue to grow up to bubbles. The rate of homogeneous nucleation can be described by the following Equation 2-1.

$$N_{homo} = C_0 f_0 exp\left(\frac{-\Delta G}{KT}\right) \tag{2-1}$$

where $N_{homo}$ is the number of nuclei generated per cm$^3$ per second. $C_0$ is the concentration of the gas (number of molecules per cm$^3$). $f_0$ is the frequency factor of the gas molecules. $K$ is the Boltzmann's constant. And $T$ is absolute temperature. The term $\Delta G$ is the "energy barrier" for homogeneous nucleation. $\Delta G$ can be calculated by Equation 2-2:

$$\Delta G = \frac{16\pi\gamma^3}{3\Delta P^2} \tag{2-2}$$

where $\Delta P$ is magnitude of the quench pressure and γ is the surface energy of the bubble interface.

The frequency factor of gas molecules in the Equation 2-1, $f_0$ , can be expressed as:

$$f_0 = Z\beta \tag{2-3}$$

where, Z, the Zeldovich factor, accounts for the fact that a large number of nuclei never grow, but rather dissolve. The rate at which the molecules are added to the critical nucleus, β, can be calculated as surface area of the critical nucleus times the rate of impingement of gas molecules per unit area. The calculation method can be expressed as Equation 2-4.

$$\beta = (4\pi r_c^3) R_{impingement} \tag{2-4}$$

Substituting Equation 2-4 into Equation 2-3:

$$f_0 = Z(4\pi r_c^3)R_{impingement} \tag{2-5}$$

Equation (2-5) shows that the frequency factor of the gas molecules joining a nucleus to make it stable varies with the surface area of the nucleus. Generally, $ZR_{impingement}$ can be regarded as a fitted parameter.

Knowing the surface energy of the system as a function of pressure and temperature, the critical size of the nuclei can be calculated at any conditions by Equation 2-6.

$$r_c = \frac{2\gamma}{\Delta P} \tag{2-6}$$

Where $r_c$ is the radius of the critical nucleus.

Equations 2-1, 2-2, 2-5, 2-6 form a complete set of the nucleation model for polymer-SCF solution.

In order to calculate the total number of nuclei generated in the system at given saturation conditions. The rate of nucleation needs to be integrated over the time period of nucleation. Generally the gas pressure falls as a function of time. Thus the starting saturation pressure ($P_{sat}$) and the pressure at which the polymer vitrifies ($P_g$) define the time scale over which the rate of nucleation should be integrated. Therefore, the total number of nuclei, $N_{total}$, can be calculated by Equation 2-7.

$$N_{total} = \int_0^t N_{homo}\,dt = \int_{P_{sat}}^{P_g} N_{homo}\frac{dP}{\left(dP/dt\right)} \tag{2-7}$$

### 2.2.3 Effect of nucleation process conditions on bubble morphology

Based on the above nucleation model, the main nucleation process parameters include saturation pressure, mixer temperature and SCF concentration. In this chapter, the effect of the three parameters and the interaction among them on the part cell morphology will be discussed.

#### 2.2.3.1 Simulation experimental model and Taguchi method

The simulation experimental model is a thin box. The size is 15.5mm×14mm×13mm. the thickness varies from 0.35mm to 1.8mm. Figure 2-2 shows the cavity distribution, gate system and cooling channels. The characteristic point position is also selected near the gate.

The PS/$CO_2$ foam system is bulit and PS brade is Vestgran 620. The each level of three process parameters are shown in the Table 2-4. Besides the studied three parameters, the initial values of other process parameters are set in the Table 2-5.

| Factors | Level1 | Level2 | Level3 |
|---|---|---|---|
| (A)Saturation pressure/ MPa | 11 | 16 | 21 |
| (B) Melt temperature/ ℃ | 220 | 240 | 260 |
| (C) Gas concentration/ % | 0.3 | 0.55 | 0.8 |

Table 2-4. Level of process parameters.

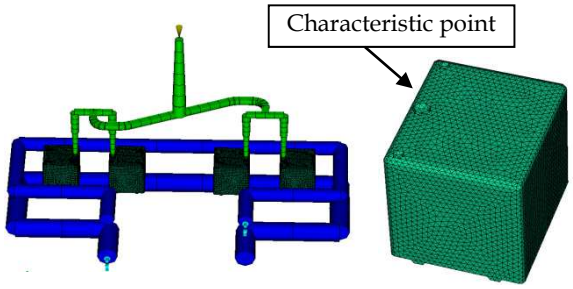


(a) (b)

Fig. 2-2. Experimental model and characteristic point position (a): CAE analysis model; (b): Characteristic point position.

| Process parameters | Value |
|---|---|
| Mold temperature/ ℃ | 50 |
| Injection time/ s | 0.6 |
| Cooling time/ s | 35 |
| Open mold time/ s | 5 |

Table 2-5. Othe rocess parameters list.

**2.2.3.2 Taguchi method**

Taguchi method is used as an experiment arrangement and parameters optimization method. Based on the setup of parameters and levels, the $L_9(3^4)$ orthogonal array is selected to arrange the experiments. Table 2-6 shows the orthogonal array. The variable analysis is used to calculate the effect order of each process parameters on the cell size and obtain the process parameters optimization combination. At the same time, the experimental results are directly analyzed, that is to calculate the average value of cell size under the three levels of the each process parameter. Here, the cell size is considered that the smaller is better. Therefore it is a minimum value issue. The calculation formula is shown as Equation 2-8 [20]:

$$m = \frac{1}{n}\sum_{i=1}^{n} y_i \tag{2-8}$$

where $m$ is the average value of process parameter under a certain level, $n$ is the number of the level, $y_i$ is the result value of the process parameter under the level. Then the difference $R_{\text{diff}}$ of each process parameter can be calculated by the maximum average value subtracting the minimum average one. Based on the $R_{\text{diff}}$ value, the effect of process parameter on the cell size can be achieved.

**2.2.3.3 Results and discussion**

*Experiment result and signal-to-noise analysis*

The simulation experiments are arranged according to $L_{27}(3^{13})$ orthogonal table. At the same time, each experiment's cell size at characteristic point is obtained. The results are shown in the Table 2-6.

| | A(MPa) | B(℃) | x1x2 | | C(%) | x1x3 | | x2x3 | | Cell Size(um) |
|---|---|---|---|---|---|---|---|---|---|---|
| 1 | 11 | 220 | 1 | 1 | 0.3 | 1 | 1 | 1 | 1 | 29.6 |
| 2 | 11 | 220 | 1 | 1 | 0.55 | 2 | 2 | 2 | 2 | 94.6 |
| 3 | 11 | 220 | 1 | 1 | 0.8 | 3 | 3 | 3 | 3 | 32.4 |
| 4 | 11 | 240 | 2 | 2 | 0.3 | 1 | 1 | 2 | 3 | 109.0 |
| 5 | 11 | 240 | 2 | 2 | 0.55 | 2 | 2 | 3 | 1 | 77.8 |
| 6 | 11 | 240 | 2 | 2 | 0.8 | 3 | 3 | 1 | 2 | 37.2 |
| 7 | 11 | 260 | 3 | 3 | 0.3 | 1 | 1 | 3 | 2 | 41.4 |
| 8 | 11 | 260 | 3 | 3 | 0.55 | 2 | 2 | 1 | 3 | 49.4 |
| 9 | 11 | 260 | 3 | 3 | 0.8 | 3 | 3 | 2 | 1 | 35.0 |
| 10 | 16 | 220 | 2 | 3 | 0.3 | 2 | 3 | 1 | 1 | 18.8 |
| 11 | 16 | 220 | 2 | 3 | 0.55 | 3 | 1 | 2 | 2 | 14.2 |
| 12 | 16 | 220 | 2 | 3 | 0.8 | 1 | 2 | 3 | 3 | 11.4 |
| 13 | 16 | 240 | 3 | 1 | 0.3 | 2 | 3 | 2 | 3 | 13.0 |
| 14 | 16 | 240 | 3 | 1 | 0.55 | 3 | 1 | 3 | 1 | 12.8 |
| 15 | 16 | 240 | 3 | 1 | 0.8 | 1 | 2 | 1 | 2 | 10.2 |
| 16 | 16 | 260 | 1 | 2 | 0.3 | 2 | 3 | 3 | 2 | 15.0 |
| 17 | 16 | 260 | 1 | 2 | 0.55 | 3 | 1 | 1 | 3 | 10.6 |
| 18 | 16 | 260 | 1 | 2 | 0.8 | 1 | 2 | 2 | 1 | 12.8 |
| 19 | 21 | 220 | 3 | 2 | 0.3 | 3 | 2 | 1 | 1 | 9.0 |
| 20 | 21 | 220 | 3 | 2 | 0.55 | 1 | 3 | 2 | 2 | 7.2 |
| 21 | 21 | 220 | 3 | 2 | 0.8 | 2 | 1 | 3 | 3 | 7.8 |
| 22 | 21 | 240 | 1 | 3 | 0.3 | 3 | 2 | 2 | 3 | 9.2 |
| 23 | 21 | 240 | 1 | 3 | 0.55 | 1 | 3 | 3 | 1 | 9.6 |
| 24 | 21 | 240 | 1 | 3 | 0.8 | 2 | 1 | 1 | 2 | 6.2 |
| 25 | 21 | 260 | 2 | 1 | 0.3 | 3 | 2 | 3 | 2 | 10.2 |
| 26 | 21 | 260 | 2 | 1 | 0.55 | 1 | 3 | 1 | 3 | 6 |
| 27 | 21 | 260 | 2 | 1 | 0.8 | 2 | 1 | 2 | 1 | 7.2 |

Table 2-6. $L_{27}(3^{13})$ Orthogonal table and experimental results.

According to Table 2-6, the S/N is calculated and the effect trend of each factors on the S/N also are gotten. Figure 2-3 shows the details. According to Figure 2-3, the significance order from big to small of the effect of each process parameters on cell size is saturation pressure (A), SCF concentration (C) and mixer temperature (B).

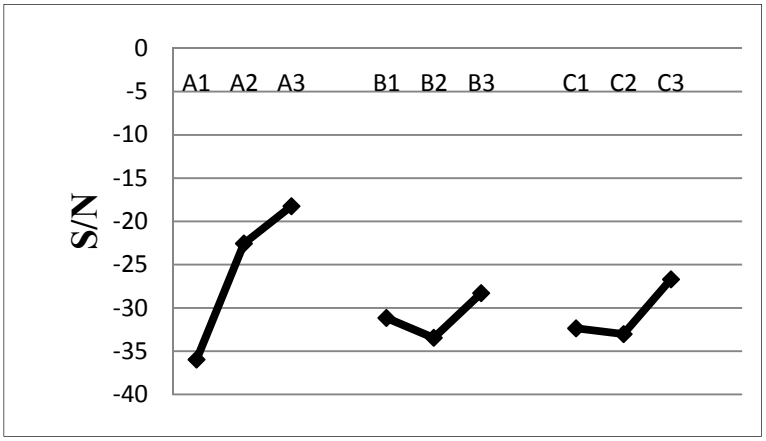


Fig. 2-3. Effect of each factors on S/N ratio.

*ANOVA analysis*

In order to further analyze the effect of each factors and the interaction among these factors on the cell morphology, ANOVA analysis is calculated according to above S/N results and experiment values. The calculation results are shown in the Table 2-7.

| | Degree of freedom | Sum of square of deviations | mean square error | F value | Significance | Significance |
|---|---|---|---|---|---|---|
| A | 2 | 12620.1 | 6310.05 | 24.1638 | 67.93% | *** |
| B | 2 | 536.500 | 268.250 | 1.02724 | 2.89% | |
| C | 2 | 912.518 | 456.259 | 1.74721 | 4.91% | Δ |
| A×B | 4 | 1158.04 | 289.510 | 1.10865 | 3.11% | |
| A×C | 4 | 6880.48 | 1720.12 | 6.58706 | 18.51% | ** |
| B×C | 4 | 979.170 | 244.792 | 0.93741 | 2.64% | |
| Error | 8 | 2089.08 | 261.135 | | | |
| Sum | 26 | 23086.8 | | | | |

Table 2-7. ANOVA analysis results.

According to Table 2-7, the conclusion of effect of saturation pressure (*A*), SCF concentration (*B*) and mixer temperature (*B*) on the cell morphology is same as the S/N results. However the interaction among the three factors is taken into account in the ANOVA analysis. Also according to Table 27, the significance order is: saturation pressure (*A*) possess 67.93%, the interaction between saturation pressure (*A*) and SCF concentration (*C*) posses 18.51%, SCF concentration (*C*) is 4.91%, Mixer temperature (*B*) is 2.89%. Compared with the S/N results, the interaction between saturation pressure (*A*) and SCF concentration (*C*) is also a very important factor to affect the cell morphology. According to F value, the effect of other factors on the cell morphology is less. So these factors belong to the error range.

Therefore, the optimization parameters combination is mainly determined by the factor *A* and *A*×*C*. Because the smaller cell size is better, the value of *A* and *B* should be the *A*3 and *B*3 in the optimization combination. Due to three levels of *C*, the *A*3×*C* combination has

three arrays. And every combination has three experimental results. The average value of each three experimental results is shown in the Table 2-8.

| | *C*1 | *C*2 | *C*3 |
|---|---|---|---|
| *A*3 | 12.53 | 9.47 | 34.86 |

Table 2-8. *A*3×*C* combination table.

According to Table 2-8, the smallest cell size is in the *A*3*C*2 array. Thus the optimization parameters combination is *A*3*B*3*C*2. And the experiment result is validated in the Figure 2-4.

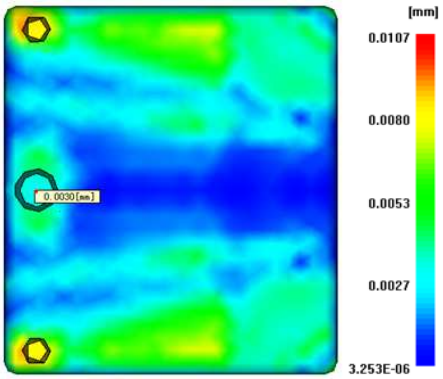


Fig. 2-4. Cell size distribution based on the optimized process parameters combination.

From the Figure 2-4, the cell radio at the characteristic point is 3 um. And the cell size on the part is between 5 um and 10 um. It means that the cell size in the part is acceptable and the distribution is reasonable. Thus the optimization parameters combination is suitable.

### 2.3 Bubble growth process

When the nucleation is completed, bubbles begin to grow up. Because the pressure of the mixer is higher than the pressure inside bubbles, SCF in the mixer diffuses into the bubbles and the bubbles grow up. Until the pressure inside the bubbles equals to the outside one or the melt is frozen, the bubbles will keep growing up.

#### 2.3.1 Classic bubble growth model

Initially, the growth and collapse of gas bubbles in both viscous Newtonian and viscoelastic non-Newtonian fluids has been investigated to research on the effect of mass transfer, and the hydrodynamic interaction between the bubble and the liquid was neglected. Barlow et al. [21] are the first to study the phenomenon of diffusion-induced bubble growth in a viscous Newtonian fluid with both mass and momentum transfer. To predict the diffusion of the dissolved gas in the viscous liquid, they used a thin shell approximation. It is assumed that the gas concentration outside the shell always remained equal to the initial concentration. The simplified diffusion equation and an analytical solution were obtained to describe the initial stage of the growth at low Reynolds numbers.

Classic bubble growth model was constructed to illustrate bubble growth in foam processing after bubble nucleation. Considered a bubble concentrically surrounded by a shell of polymer melt with a constant mass, the gas dissolved in the melt shell uniformly distributes in a saturation state at the initial time and only diffuses between the melt shell and the bubble during bubble growth. Figure 2-5 shows the configuration of the bubble and the melt shell surrounding the bubble. The spherical coordinate is selected with the center of the bubble as the origin. In Figure 2-5, $R$ is the bubble radius, $S$ is the outer radius of the melt shell, and $c$ is the concentration of the dissolved gas in the mixer.

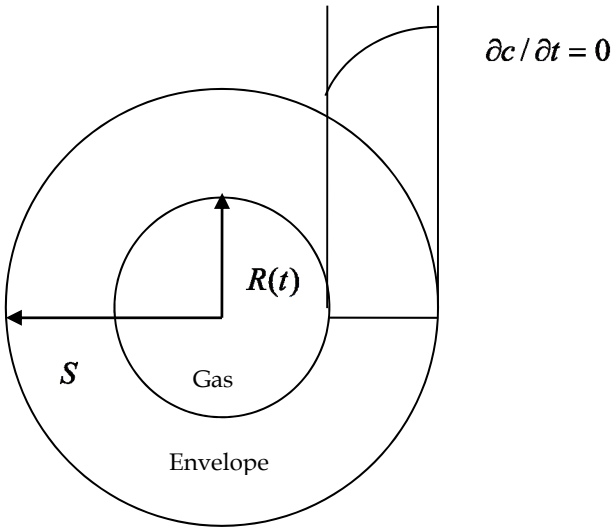


Fig. 2-5. Schematic of the unit cell model.

Before analyzing the bubble growth, the following assumptions are made.

1. Bubble and melt shell have the same and fixed sphere center during the bubble growth.
2. The gravity and inertia effects are ignored because of the highly viscous polymer melt.
3. The polymer melt is incompressible. The volume of dissolved gas in the melt is ignored.
4. Because the timescale of the bubble expansion is much shorter than the cooling time, the growth process is considered to be isothermal.
5. The dissolved gas in the polymer melt is in the uniformly supersaturated state before bubble growth.
6. The dissolved gas does not go in and out at the outer boundary of the analyzed region.

At the same time, it is also assumed that the cell shape is spherical, the initial radius is $R_0$ ,the internal gas pressure $P_{g0}$ equals to the melt plasticization pressure and the gas in the cell is ideal gas. Thus the change rate of the radius of the cell, $R$ , is controlled by Equation 2-9 [22]:

$$\frac{\mathbf{d}R}{\mathbf{d}t} = \frac{1}{4\eta}\left[\left(P_{\mathrm{g}} - P\right)R - 2\sigma\right] \tag{2-9}$$

where $\eta$ is the melt viscosity, $P_g$ is the gas pressure in the micro-cell, $\sigma$ is the surface tension at the interface of the melt and the gas, $P$ is the pressure of the melt at the outer boundary of the cell.

**2.3.1.1 Gas diffusion**

Based on the dynamics principle of cell model, the value of $P_g$ decreases when $R$ becomes larger. At the same time, the gas only diffuses into the cell. The gas diffusion is determined by the gas dissolution grads. The diffusion will be going on until the driven power disappears or the melt is frozen. Thus, the relationship between $R$ and $P_g$ can be governed by Fick´s law of diffusion:

$$\frac{\partial c}{\partial t} + v_r \frac{\partial c}{\partial r} = D\left[\frac{1}{r^2}\frac{\partial}{\partial r}\left(r^2 \frac{\partial c}{\partial r}\right)\right] \quad \text{R(t)≤r≤S} \tag{2-10}$$

where $c$ is the concentration of the dissolved gas in the mixer, $v_r$ is the gas diffusion velocity in the radius direction of spherical coordinates, $D$ is the diffusion coefficient in the single solution, $r$ is the radial coordinate, $t$ is the time, $S$ is the radius of the cell.

The left of Equation 2-10 shows the change rate of gas concentration, while the right shows the gas mass diffusion. Where $v_r$ can be estimated by Equation 2-11 [22]:

$$v_r = \frac{R^2}{r^2}\frac{\mathbf{d}R}{\mathbf{d}t} \tag{2-11}$$

when $t = 0$, $c(r, t = 0) = c_0$.

It assumes that the cell size in the same area is consistent. Thus,

when $r = S$: $\frac{\partial c}{\partial r} = 0$.

And the gas concentration $c$ between $S$ and $R(t)$ can be calculated by Henry law:

$$c(R,t) = k_h P_g(t) \ , \tag{2-12}$$

where $k_h$ is the Henry law coefficient. It is determined by the plastics and gas type and governed by Equation 2-13:

$$\ln k_h = -2.1 + 0.0074 T_{cr} \ , \tag{2-13}$$

where $T_{cr}$ is the critical temperature.

As said above, the gas in the cell is assumed as ideal gas. Thus $P_g(t)$ can be calculated by Equation 2-14 [23]:

$$P_g(t) = \left[1000 R_g T \Big/ M_w\right] \rho_g(t) = A \rho_g(t) T \tag{2-14}$$

where $R_g$ is gas constant, $R_g = 8.3145\ \mathrm{J/(mol \cdot K)}$, $T$ is the temperature (K), $M_w$ is gas molecular weight, $\rho_g$ is the gas density in the cell. Here $A = 1000 R_g / M_W$, thus $A$ is constant for a certain gas.

The gas diffusion coefficient $D$ in the Equation 2-10 can be calculated by Equation 2-15:

$$D = df_1 \exp(\frac{df_2}{T}) \tag{2-15}$$

where $T$ is the temperature, $df_1$ and $df_2$ are given coefficients.

#### 2.3.1.2 Material properties

The melt viscosity $\eta$ can be proposed by Cross-WLF model. Thus the melt viscosity $\eta$ in the Equation 2-9 can be expressed by Equation 2-16 [23]:

$$\eta(T,\dot{\gamma},p) = \eta_0(T,p) f(\phi) \left[ 1 + \left( \frac{\eta_0 \dot{\gamma}}{\tau^*} \right)^{(1-n)} \right]^{-1} \tag{2-16}$$

where $\eta$ is the viscosity of the polymer-gas single solution, $T$ is the temperature, $\dot{\gamma}$ is the shear rate, $p$ is the pressure, $n$ is the power coefficient, $\tau^*$ the critical shear stress, $\eta_0(T,p)$ is the viscosity under zero shear rate. Because SCF is added into the melt, the effect of SCF on the plastics viscosity can be expressed by $f(\phi)$ . The following equation can be used to describe $f(\phi)$ [23]:

$$f(\phi) = (1-\phi)^{\alpha} \tag{2-17}$$

where $\alpha$ is an empirical constant. here $\alpha = 2$ . $\phi$ is the volume fraction of the gas. It can be calculated by Equation 2-18:

$$\phi = \frac{4\pi R^3 / 3}{1/(\rho N_{\mathbf{m}}) + 4\pi R^3 / 3} \tag{2-18}$$

where $N_{\mathbf{m}}$ is the cell number in unit volume.

The surface tension $\sigma$ at the interface between melt and gas in the Equation 2-9 can be calculated by Equation 2-19 [22]:

$$\sigma(T) = \sigma(298) \left( \frac{\overline{\rho}}{\overline{\rho}(298)} \right)^4 \tag{2-19}$$

where $\sigma(298), \sigma(T)$ are the surface tensions at the room temperature and at process temperature respectively, and $\overline{\rho}(298), \overline{\rho}$ are the densities of the single solution at the room temperature and at process temperature respectively.

### 2.3.2 Effect of process conditions on bubble morphology

#### 2.3.2.1 Simulation experimental model

Based on the above mathematic model, the pre-filled volume, initial cell diameter, cell density and SCF concentration are necessary as boundary conditions besides the process

parameters required by traditional injection process simulation. Finite element method and finite difference method are combined to solve the equations. To ensure the accuracy of simulation results, plastics properties used in the simulation must be recalculated based on the material model described in the "Material properties" section.

**2.3.2.2 Simulation experimental model**

A flat part, with the size of 320mm×280mm×2mm, is selected for simulation. Figure 2-6 shows the part geometries, gate and cooling systems. As known from the former research, the difference of cell size near the gate between the true value and simulation result is smaller. So the characteristic point near the gate is selected to study the effect of process parameters on the cell size. The position is also shown in the Figure 2-6.

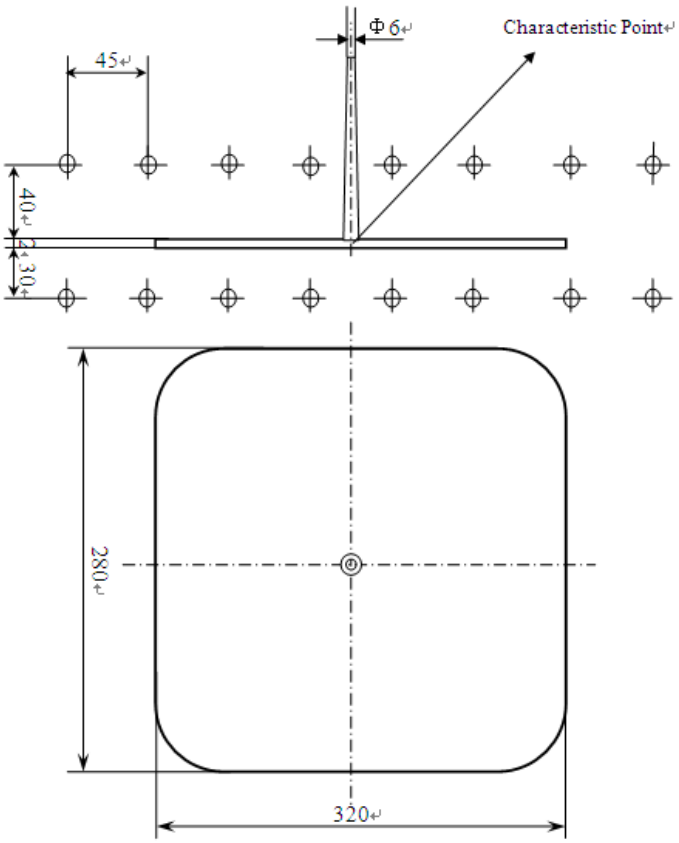


Fig. 2-6. Experiment model.

Polypropylene material is used in the simulation. Its main properties are shown in Table 2-9. Nitrogen is used as blow agent. Its main properties are as follows. $M_w = 28$, $\sigma(298) = 5 \times 10^{-5}$ **N/mm**, $kh_1 = 1.346 \times 10^{-9}$, $kh_2 = -1.709 \times 10^{5}$, $df_1 = 3.819 \times 10^{-7}$, $df_2 = -2803.5$ [24].

| Main properties | Value |
|---|---|
| Eject temperature /℃ | 122 |
| Max. melt temperature /℃ | 250 |
| Special heat /J/kg•℃ | 3531 |
| Thermal conductivity /W/m•℃ | 0.17 |
| Melt density /g/cm$^3$ | 0.814 |

Table 2-9. Polypropylene properties.

The effect of mold and melt temperatures, injection time and pre-filled volume on the cell size is studied. Based on the cooling and gate systems, recommended material parameters and the initial simulation results, the selected levels for each process parameter are shown in Table 2-10. Besides the studied four parameters, the initial values of other parameters are set as the following. nucleation density $\rho = 2 \times 10^{11}$ **/m$^3$**, initial gas concentration $c_0 = 0.25\%$, initial cell radius $R_0 = 1.0 \times 10^{-6}$ m [25].

**2.3.2.3 Results and discussion**

The $L_9(3^4)$ orthogonal array is used to arrange the simulation experiments. The cell sizes values at the characteristic point are calculated. Table 2-10 shows the experiment arrangement order and the simulation results. Based on the Equation 2-8, the average values of each process parameter at each level are calculated. The $R_{diff}$ values are also achieved after the max. and min. average values are gotten. Table 2-11 shows the details.

| No. | Column | | | | Mold temp. (℃) | Melt temp. (℃) | Inj. time (s) | Pre-filled vol. (%) | Cell size (um) |
|---|---|---|---|---|---|---|---|---|---|
| | 1 | 2 | 3 | 4 | | | | | |
| 1 | 1 | 1 | 1 | 1 | 10 | 180 | 1 | 85 | 28 |
| 2 | 1 | 2 | 2 | 2 | 10 | 210 | 1.5 | 90 | 43 |
| 3 | 1 | 3 | 3 | 3 | 10 | 240 | 2 | 95 | 40 |
| 4 | 2 | 1 | 2 | 3 | 20 | 180 | 1.5 | 95 | 25 |
| 5 | 2 | 2 | 3 | 1 | 20 | 210 | 2 | 85 | 47 |
| 6 | 2 | 3 | 1 | 2 | 20 | 240 | 1 | 90 | 42 |
| 7 | 3 | 1 | 3 | 2 | 30 | 180 | 2 | 90 | 34 |
| 8 | 3 | 2 | 1 | 3 | 30 | 210 | 1 | 95 | 37 |
| 9 | 3 | 3 | 2 | 1 | 30 | 240 | 1.5 | 85 | 47 |

Table 2-10. $L_9(3^4)$ orthogonal array, experiment arrangement and results.

| | Mold temp. (℃) | Melt temp. (℃) | Inj. time (s) | Pre-filled vol. (%) |
|---|---|---|---|---|
| $m_1$ | 37.0 | 29.0 | 35.7 | 40.7 |
| $m_2$ | 38.0 | 42.3 | 38.3 | 39.7 |
| $m_3$ | 39.3 | 43.0 | 40.3 | 34.0 |
| $R_{diff}$ | 2.3 | 14.0 | 4.6 | 6.7 |

Table 2-11. Direct analysis of process parameters.

According to Table 2-11, the effect of process parameters on the cell size is showed in the Figure 2-7.

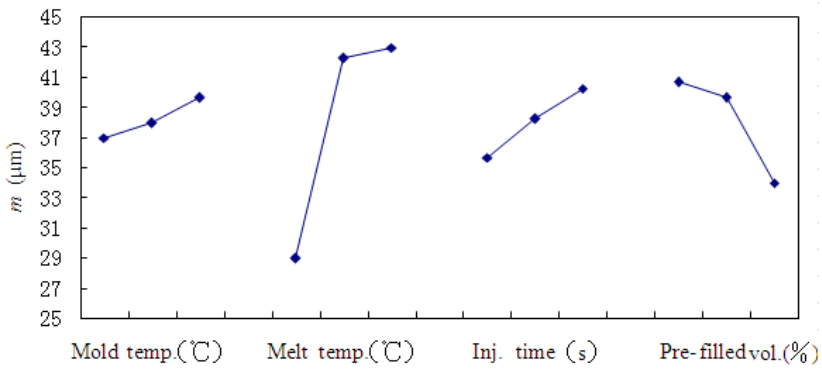


Fig. 2-7. Effect of each process parameter on cell size.

According to the $R_{diff}$ values in Table 2-11, the effect order from big to small of each process parameter on the cell size is melt temperature, pre-filled volume, injection time and mold temperature and the optimization parameters combination is mold temperature(10℃), melt temperature(180℃), injection time(1s) and pre-filled volume(95%). Based on the above combination, the cell size distribution is shown in Figure 2-8. The cell radius at the characteristic point is 7 μm and the cell size in whole part is between 5μm and 40μm. The smaller cell size can avoid some part defects such as dimples etc. Obviously this cell size distribution can be accepted.

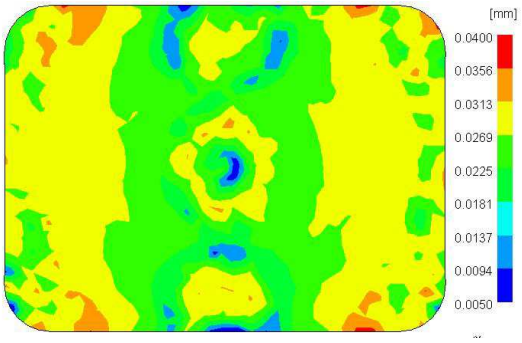


Fig. 2-8. Cell size distribution.

According to Figure 2-7, appropriately reducing the melt temperature and increasing the pre-filled volume can optimize the cell size. However the effect of injection time and mold temperature on cell size was less significant. In order to further research the effect trend of each process parameters on the cell size. More simulation experiments are done. Because the mutually effect among the selected process parameters is not taken into account, the further research is done by adjusting one of the four parameters and fixing the other parameters.

When one of the four parameters is studied, other parameters are set according to the optimization result. Table 2-10 shows the adjusted values of each parameter. So the effect trend of melt temperature, pre-filled volume, injection time and mold temperature on the cell size are achieved. Figure 2-9 shows the effect trend.

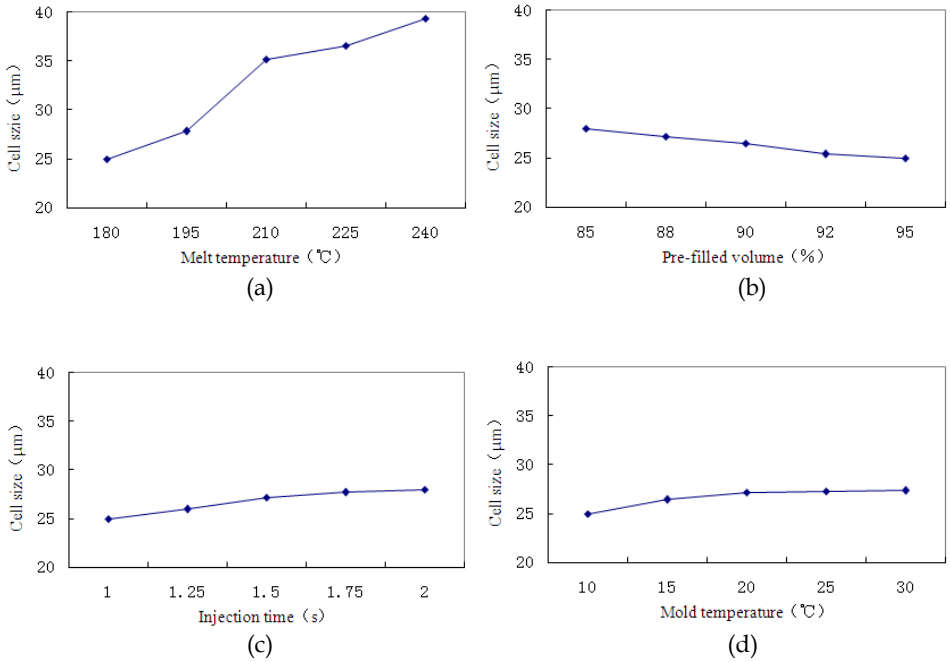


Fig. 2-9. Effect trend of each process parameters on cell size (a) melt temperature; (b) pre-filled volume; (c) injection time; (d) mold temperature.

According to Figure 2-9 (A), cell size changes largely along with temperature drop. Because of the lower melt temperature, the cooling time is shorter and the cell growth time also becomes shorter. The cell size becomes smaller. At the same time, due to the shorter cooling time, the cell growth can be controlled easily. Thus the smaller and evener cell size can be produced. With the pre-filling volume increasing, the foaming space becomes smaller. At the same time, the number of nucleation points per volume is certain. So the cell size becomes smaller. However, on the other hand, the more part weight can not be reduced with the pre-filled volume increasing. Figure 2-9 (B) shows the cell size change trend along with the pre-filled volume change. When the injection time is increased, the cell growth time also becomes longer. Thus the cell size becomes bigger. However Figure 2-9(C) shows the effect of injection time on the cell size is inferior to melt temperature and pre-filled volume. At last, according to the mathematic model of cell growth, the effect of mold temperature on the cell size is little. Figure 2-9 (D) also shows that the cell size changes little with mold temperature decreasing.

## 3. Microcellular foam injection molding products surface defects and solutions

As said in above chapter, microcellular foam injection molding parts have many advantages such as saving material and energy, reducing cycle time, and parts excellent dimensional stability. Despite these advantages, the low parts' surface quality limits its application scope seriously. Typical defects are swirl marks, silver streak, surface blistering, post-blow, large surface roughness. The details are introduced on above chapter.

### 3.1 Technologies to improve surface quality

Until now, many technologies for improving surface quality have been studied. The typical technologies include Gas Counter Pressure (GCP), Rapid Heating Cycle Molding (RHCM) and Film Insulation which is derived from RHCM.

**Gas Counter Pressure (GCP)**

When polymer-SCF mixer is injected into the cavity, counter pressure can prevent bubbles growth due to the high cavity pressure. When the injection is completed, the high cavity pressure is released, and then the bubbles begin to grow up. However, the surface melt has solidified at that time. So the parts surface quality can be as satisfied as traditional injection parts'.

GCP method can control the bubbles growth and remove the swirl marks. But it is not suitable for mass production due to the complex mold structure and high cost.

**Rapid Heating Cycle Molding (RHCM)**

Compared with conventional injection molding process, RHCM process is that the mold is rapidly heated before filling stage. The heated mold temperature is higher than the polymer thermal deformation temperature. Then the filling and packing process are going. Afterward, the mold is rapidly cooled. Finally, the products are ejected from the mold. So RHCM process circle is finished [18].

RHCM technology is widely used to improve the surface quality of injection molding parts. For example, to improve optical transparence and decrease birefringence of polystyrene, radiation heating on injection mold is proposed to directly control the temperature during the filling stage. A polycarbonate lens with a variation thickness from 1.5 mm to 7 mm can be successfully produced by electric heaters combined with chilly water cooling method.

Previous discussions about microcellular foam injection parts surface defects show that the melt temperature on the cavity surface affects the parts surface quality obviously. RHCM can meet the temperature requirement. On Oct., 2010, Trexel Inc., the supplier of the MuCell microcellular foaming technology, announced to promote MuCell for injection molding parts with Class-A/high-gloss surface finish at a global licensing agreement with Ono Sangyo Co. Ltd.. Chen SC and Li HM has successfully demonstrated the usefulness of a variable mold temperature in improving parts surface quality during microcellular foam injection molding process [14]. Figure 3-1 shows their experimental results.

Figure 3-2 shows that the effect of mold temperature on the surface roughness is very insignificant when the mold surface temperature is below 100℃. The surface roughness

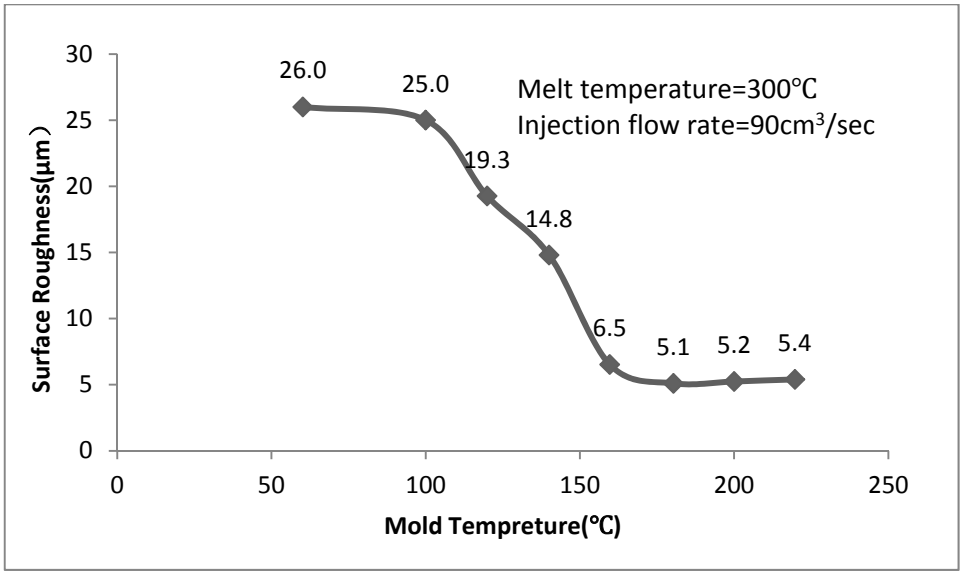


Fig. 3-1. Effect of mold temperature on the surface roughness of microcellular foam injection molded parts [26].

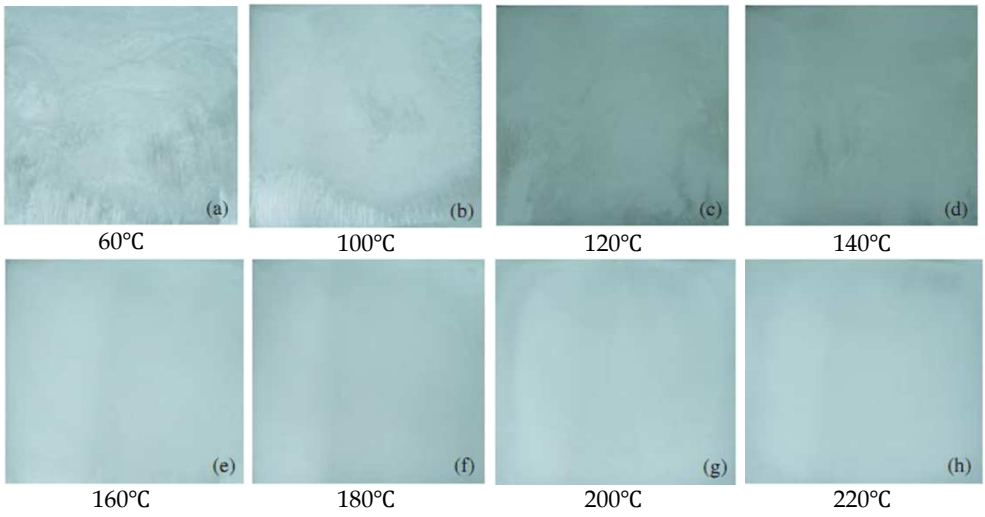


Fig. 3-2. Surface visual quality molded under different mold temperatures [26].

decreases from 25μm to 6.5μm when the mold surface temperature increases from 100℃ to 160℃. When the mold temperature reached a critical value of approximately 180℃, the surface roughness begins to level off at 5μm.

Figure 3-2 reveals that visible surface flow marks were eliminated with the mold temperatures higher than 160℃. The reason is that when the temperature of the polymer-

SCF mixer is higher than its glass transition temperature or the melting point (140℃ for the PC resin), gas bubbles flow marks do not form on the surface of the microcellular foam injection parts. So to improve the microcellular foam injection surface quality, RHMC process is one of useful methods.

**Film insulation**

RHCM technology can evidently improve the surface quality, but the heating equipment is necessary and complicated and the mold should be surface finish, good corrosion resistance and excellent hot strength. These will lead to more cost. Based on the theory of RHCM, the insulated films is stick on the surface of mold core to control the melt temperature on the cavity surface. This method is called Film Insulation. At present, the reported materials that can be used as insulation film include PEEK, PTFE, PET/PC, and so on[27-28].

Polymer film (82%PET+18%PC) is used as insulated film to improve surface quality. Table 3-1 is the experiment results [14].

| Film thickness [mm] | Surface roughness [μm] | Improved efficiency [%] |
|---|---|---|
| 0 | 26 | 0 |
| 0.125 | 5.6 | 78 |
| 0.188 | 1.8 | 93 |

Table 3-1. Surface toughness and improved efficiency under different thicknesses of films used for molding [14].

Table 3-1 shows that the surface roughness decreases obviously from 5.6μm to 1.8μm when the film layer thickness increases from 0.125mm to 0.188 mm. Compared with parts molded at mold temperature of 60 ℃ without film layer, the surface quality can be greatly improved without a significant cycle time increase.

PTFE insulated film is also used [29]. And the experiment results in terms of surface roughness, surface profile of conventional and microcellular injection molded parts with and without the insulated film are discussed. Table 3-2 shows the thermal analysis of the corresponding microcellular foam injection molding experiments.

| Thickness of PTFE [μm] | Interfacial Temperature [°C] | Heat Fluxes [kW/m$^2$] |
|---|---|---|
| 75 | 59 | 113 |
| 125 | 76 | 102 |
| 175 | 90 | 93.5 |
| 225 | 104 | 85.8 |

Table 3-2. Predicted interfacial temperatures and heat fluxes with different thickness of PTFE [29].

The experiment results show that the swirl marks are eliminated under the condition of the film thickness bigger than 175μm. Because of the excellent properties about low thermal conductivity ($k$=0.25W/( m·K)), low coefficient of friction(<0.1) and high melting point (327℃), PTFE is very suitable to be used as insulated film.

Film Insulation method makes the interfacial temperature with a thin layer of insulated film higher than that of the conventional injection mold. These results show that Film Insulation is as acceptable as RHCM.

## 4. Summary

In this chapter, microcellular foam injection molding process is introduced. Based on the analysis of the characters of microcellular foam injection molding process, the nucleation theory and bubble growth model are described. Then the effect of process parameters on the cell morphology is detailed studied. At last, the part surface defects of microcellular foam injection molding process are introduced. At the same time, the methods to overcome such defects are referred.

## 5. References

[1] Kelvin T. Okamoto. Microcellular Processing [M]. Cincinnati: Hanser Gardner publications Inc., 2003

[2] University of Washington, Microcellular Plastics Lab. [online] Available: http:// faculty. washington.edu/ vkumar/microcel/

[3] Zhai Wentao,Yu Jian,He Jiasong. Research progresses in preparation of microcellular polymers by supercritical fluid technique [J]. Chinese polymer bulletin. 2009, 3: 1-10

[4] Hyde LJ, Kishbaugh LA. The MuCell® Injection Molding Process: A Strategic Cost Savings Technology for Electronic Connectors[C]. Trexel Inc, IICIT Annual symposium, USA, 2003

[5] Bill N, Mark B. The Supercritical Fluid (SCF) Delivery System[J/OL]. Trexel. Inc

[6] Williams JM, Wrobleski DA. Microstructures and properties of some microcellular foams [J]. Journal of materials science, 1989, 24 (11):4062-4067

[7] Matuana LM, Park CB, Balatinecz JJ. Structures and mechanical properties of microcellular foamed polyvinyl chloride [J]. Cellular polymers, 1998, 17(1): 1-16

[8] Kumar V, Juntunen RP, Barlow C. Impact strength of high relative density solid state carbon dioxide blown crystallizable poly(ethylene terephthalate) microcellular foams [J]. Cellular polymers. 2000, 19(1): 25-37

[9] Ozkul MR, Mark JE, Aubert JH. Elastic and plastic mechanical responses of microcellular foams [J]. Journal of applied polymer science. 1993, 48(5): 767-774

[10] Ozkan E. Thermal and mechanical properties of cellular polystyrene and polystyrene and polyurethane insulation materials aged on a flat roof in hot-dry climate [J]. Journal of testing and evaluation, 1994, 22(2): 149-160

[11] Nimmer RP, Stokes VK, Ysseldyke DA. Mechanical properties of rigid thermoplastic foams-Part II: Stiffness and strength data for modified polyphenyleneoxide forms [J]. Polymer engineering and science. 1988, 28(22): 1501-1508

[12] Progelhof RC, Kumar S, Throne JL. High speed puncture impact studies of three low pressure styrene thermoplastic structural foam plaques [J]. Advances in polymer technology. 1983, 3(l): 15-22

[13] Yin Z, Heath RJ, Hourston DJ. Morphology, mechanical properties, and thermal stability of polyurethane-epoxide resin interpenetrating polymer network rigid foams [J]. Journal of applied polymer science. 2000, 75(3): 406-416

[14] Chen Shiachung, Li Haimei, Hwang Shyhshin, *et al*. Passive mold temperature control by a hybrid filming-microcellular injection molding processing [J]. International Communications in Heat and Mass Transfer.2008, 35: 822–827

[15] Hu Guanghong: Research on key technologies of microcellular foam injection molding process [D]. Shanghai: Shanghai Jiao Tong University, 2009

[16] Yoon JD, Hong SK, Kim JH, et al. A mold surface treatment for improving surface finish of injection molded microcellular parts [J]. Cellular polymer, 2004, 23(1): 39–47

[17] Zhang Yatao, Li Haimei, Hwang Stanley, et al.Surface Defects and Morphology of Microcellular Injection Molded PC Parts [J].Polymer materials science & engineering. 2010, 4: 127-130

[18] Wang Yuea, Hu Guanghong.Research progress of improving surface quality of microcellular foam injection parts [J]. Applied Mechanics and Materials. 2011, 66-68: 2010-2016

[19] Goel SK, Beckman EJ. Generation of microcellular polymeric foams using supercritical carbon dioxide. I: Effect of pressure and temperature on nucleation [J]. Polymer engineering and science, 1994, 34(14): 1137-1147

[20] Fang Kaitai, Orthogonal and Symmetrical Experiment Design [M]. Beijing: Scientific Publishing House, 2001: 1-17 (in Chinese).

[21] Barlow EJ, Langlois WE. Diffusion of Gas from a Liquid into an Expanding Bubble [J]. Journal of Research and Development. 1962, 6(3): 329-337

[22] Han S J, Kennedy P, Zheng R, *et al*, Numerical analysis of microcellular injection molding [J], Journal of Cellular Plastics, 2003,39(11):475-485.

[23] Gramann P, Turng L S, Chandra A *et al*, Modeling cell nucleation during microcellular injection molding [C]. SPE's Annual Technical Conference, Wisconsin, 2003:569-575.

[24] Moldflow Pty. Ltd. Moldflow Plastics Insight Training Manual [M]. Moldflow Pty. Ltd , USA, 2003.

[25] Osorio A, Turng L S, Mathematical modeling and numerical simulation of cell growth in injection molding of microcellular plastics, [J] Polymer Engineering Science, 2004 ,44(12): 2274-2286.

[26] Chun Shiachuang, Lin Yuwan, Chien Reander, *et al*. Variable Mold Temperature to improve Surface Quality of microcellular injection molded parts using induction heating technology [J].Advances in polymer technology.2008, 27(4): 224–232

[27] Takada M, Tanigaki M, Ohshima M. Effects of CO2 on crystallization kinetics of polypropylene [J]. Polymer Science and Engineering. 2001, 41(11): 1938-1946

[28] Turng LS, Kharbas H. Development of a hybrid solid-microcellular co-injection molding process [J] International polymer processing. 2004, 19(1): 77-86

[29] Chen Huili, Chien Reander, Chen Shiachung. Chen.Using thermally insulated polymer film for mold temperature control to improve surface quality of microcellular injection molded parts [J].International Communications in Heat and Mass Transfer. 2008, 35: 991-994

[30] Wikipedia, the free encyclopedia. Supercritical fluid. [online] Available: http://en.wikipedia. org/wiki/Supercritical_fluid
[31] Colton J.S,The nucleation of microcellular thermoplastic foam[D]. Massachusetts: MIT, 1985.

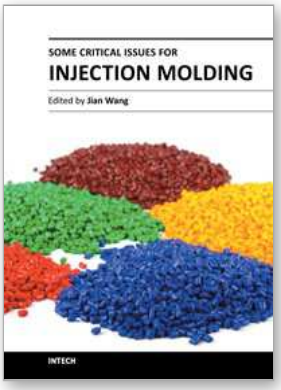


**Some Critical Issues for Injection Molding**

Edited by Dr. Jian Wang

ISBN 978-953-51-0297-7
Hard cover, 270 pages
**Publisher** InTech
**Published online** 23, March, 2012
**Published in print edition** March, 2012

This book is composed of different chapters which are related to the subject of injection molding and written by leading international academic experts in the field. It contains introduction on polymer PVT measurements and two main application areas of polymer PVT data in injection molding, optimization for injection molding process, Powder Injection Molding which comprises Ceramic Injection Molding and Metal Injection Molding, ans some special techniques or applications in injection molding. It provides some clear presentation of injection molding process and equipment to direct people in plastics manufacturing to solve problems and avoid costly errors. With useful, fundamental information for knowing and optimizing the injection molding operation, the readers could gain some working knowledge of the injection molding.



INTECH
open science | open minds

**InTech Europe**
University Campus STeP Ri
Slavka Krautzeka 83/A
51000 Rijeka, Croatia
Phone: +385 (51) 770 447
Fax: +385 (51) 686 166
www.intechopen.com

**InTech China**
Unit 405, Office Block, Hotel Equatorial Shanghai
No.65, Yan An Road (West), Shanghai, 200040, China
中国上海市延安西路65号上海国际贵都大饭店办公楼405单元
Phone: +86-21-62489820
Fax: +86-21-62489821